



## Hotspots in Photovoltaic Arrays Based on Multipoint Parabolic Motion



Zhikai Dai<sup>①</sup>, Gong Chen<sup>\*②</sup>, Zhiqi Chen<sup>③</sup>, Chang Lu<sup>④</sup>, Yao Zheng<sup>⑤</sup>, Xinyi Wang<sup>⑥</sup>, Jinqiu Wang<sup>⑦</sup>, Rui Min<sup>⑧</sup>, Xinyang Wu<sup>⑨</sup>, Wei Wei<sup>⑩</sup>, Zhengpeng Yang<sup>⑪</sup>, Deyi Li<sup>⑫</sup>, Huachao Zhang<sup>⑬</sup>, Ziyu Yang<sup>⑭</sup>, Yeshuai Shao<sup>⑮</sup>

College of Electrical and Information Engineering, Changzhou Institute of Technology, 213000 Changzhou, China

\* Correspondence: Gong Chen (chengong@czu.cn)

Received: 07-27-2025

Revised: 09-03-2025

Accepted: 09-11-2025

**Citation:** Z. K. Dai, G. Chen, Z. Q. Chen, C. Lu, Y. Zheng, X. Y. Wang, J. Q. Wang, R. Min, X. Y. Wu, W. Wei, Z. P. Yang, D. Y. Li, H. C. Zhang, Z. Y. Yang, and Y. S. Shao, "Hotspots in photovoltaic arrays based on multipoint parabolic motion," *Math. Model. Sustain. Eng.*, vol. 1, no. 1, pp. 35–47, 2025. <https://doi.org/10.56578/mmse010103>.



© 2025 by the author(s). Licensee Acadlore Publishing Services Limited, Hong Kong. This article can be downloaded for free, and reused and quoted with a citation of the original published version, under the CC BY 4.0 license.

**Abstract:** With the rapid development of solar power generation technology, the hotspot effect of photovoltaic (PV) arrays poses a key challenge to the efficiency and stability of the system. Conventional PV array models have significant limitations in dealing with complex shadow shading and multi-peak output characteristics, especially when confronted with complex topologies such as the complex-total-cross-tied (CTCT) structures. To address this issue, this paper proposed a mathematical model for PV arrays based on multipoint parabolic motion, which could accurately simulate the output characteristics of PV arrays under localized shading conditions. The model decomposed the current-voltage ( $I - V$ ) characteristic curve of the PV arrays into multiple parabolic trajectories. A shadow shading model for complex structures was successfully constructed by combining with a kinematic model. MATLAB/Simulink simulations and experimental validation showed that the proposed model guaranteed computational accuracy with error less than 5%, while computational efficiency was greatly improved. The proposed model could accurately capture the multi-peak characteristics when compared with the traditional engineering model. Results from the experiment further verified the robustness of the model in dynamic shading scenarios, hence providing an efficient and reliable tool for maximum power tracking and hotspot localization in the PV system.

**Keywords:** Hotspot; Shadow shading model; Translational motion; Photovoltaic arrays

### 1 Introduction

In recent years, power generation with solar energy, an emerging green energy source, has achieved rapid development and become one of the most promising alternative energy sources in the 21st century. In practice, due to environmental and other factors, the light received by the photovoltaic arrays is not uniform, and even some parts of the array will be blocked so that the photovoltaic (PV) hotspot will be generated, thus affecting the output characteristics of the PV system. Therefore, the detection of PV modules through the process of its production, application, and repair has become a hotspot of current research and an important issue that cannot be ignored [1]. To realize the detection of PV modules, it is necessary to study the electrical output characteristics of PV monoliths as well as PV arrays, i.e., a suitable PV array model. The model is used to analyze and diagnose hotspot failures and provide timely remediation, based on the severity of shadow shading.

At present, domestic and international research on photovoltaic panel modeling is gradually expanding from basic theory to complex scenarios. Wang and Bian [2] proposed an engineering mathematical model and a simulation model for the PV panels, which can accurately reproduce external output characteristics of the PV cells and their arrays under certain engineering environments, only according to the attribute parameters  $I_{sc}$ ,  $V_{oc}$ ,  $I_m$ , and  $V_m$  provided on the relevant PV panels. Yet, it does not take into account the effect of shading. Shao et al. [3] systematically analyzed the performance of various PV array configurations under dynamic shading, and pointed out that the traditional series-parallel structure (SP) could be used for energy generation under dynamic shading. While electrical array reconfiguration (EAR) could optimize the performance, it still relied on hardware topology adjustment and could not respond to instantaneous shading changes in real time. In contrast, the model in this paper could directly achieve real-time parameter adjustment under dynamic shading through mathematical modeling without hardware

reconfiguration, which significantly improved the computational efficiency. Kim et al. [4] proposed a low-complexity maximum power point tracking algorithm, which simplified the computational steps but still required iterative optimization, and its real-time performance was limited. The model in this paper used analytical expressions to directly calculate the output characteristics under dynamic shadowing; it was suitable for online monitoring and control as it avoided the complex optimization process. Li et al. [5] and others proposed a hotspot detection method based on distributed fiber Bragg grating sensors. Although it could achieve high-precision temperature monitoring, it relied on the physical sensor hardware only, and did not incorporate multi-physical field dynamic parameters, such as light intensity, temperature, and so on. In this paper, we innovatively coupled light intensity, temperature, and real-time shadow trajectory to achieve the synergistic optimization of multi-physical fields by dynamically adjusting the model parameters to solve the dependence on a single factor in traditional methods.

Regarding the limitations of shading occlusion modeling, Shao et al. [3] further pointed out that although the traditional physical array reconstruction (PAR) and electrical array reconstruction (EAR) techniques could optimize the performance under dynamic shading, both of them required hardware tuning or sensor support, which led to an increase in the cost of the system. El Iysaouy et al. [6] analyzed four types of typical partial shading patterns and proposed a fast-modeling method for photovoltaic arrays under shading conditions, but this study did not consider the relevant situations of photovoltaic arrays with complex structures under shading conditions. Pei and Hao [7] proposed a localized shading model based on dynamic light intensity adjustment, which could adapt to real-time shading variations, but did not consider the adaptability of complex topologies (e.g., complex-total-cross-tied (CTCT)). Chanchangi et al. [8, 9] analyzed the effect of ash accumulation on the output power of PV modules, and the model was only applicable to a single type of shading. They did not cover the dynamic shading or the interaction effect of complex topological structures. Almarri et al. [10] investigated the interference of multi-factor coupling such as humidity and sand/gravel on the output characteristics of photovoltaic modules, but did not improve the shading model related to ash accumulation. Parvin et al. [11] proposed an error prediction troubleshooting method that could capture the dynamic response of shading but relied on recurrent neural network (RNN) training, which had limited real-time and high computational resource requirements. Tai et al. [12] analyzed the effect of local shadows based on a single diode equivalent circuit, but the model was not adapted to complex structures, such as CTCT. The computational complexity was significantly increased due to the inclusion of exponential/logarithmic operations. Although the reconstruction strategy proposed by Zhu et al. [13] optimized the output power through the 0–1 multiple backpack problem, it relied on the principle of irradiance equalization and did not consider the dynamic adjustment of voltage distribution. In the above introduction, it can be found that there are still some problems to be improved in the current research on PV modules. The model in this paper provided insights into the study of PV modules and focused on solving these problems. The model in this paper avoided exponential/logarithmic operations through the parabolic motion segmented analysis. The computational efficiency was greatly improved while supporting the accurate modeling of complex topologies such as CTCT, coupling with multi-physical field parameters (light, temperature, and shading trajectory) to achieve dynamic optimization. Unquantified multi-peak errors under shading conditions may fail at high occlusion rates. Existing hotspot detection techniques mostly rely on infrared thermal imaging [14], which can locate faults but require complex hardware support and high cost. This paper proposed models to reduce the dependence on physical sensors through mathematical modeling.

Having synthesized the analysis from the above literature, the existing photovoltaic hotspot model has limitations such as a large arithmetic capacity and a small scope of application. In this paper, based on the engineering model of photovoltaic cells [2] combined with the kinematic model of photovoltaic cells [11], we simulated the formation of hotspots by analyzing the relationship between the output voltage and current of PV arrays, and the output voltage and power. We constructed the photovoltaic hotspot fault model based on the multipoint parabolic motion under the local shadow shading and compared it with the engineering model.

## 2 Modeling of PV Arrays under Shadow Masking

### 2.1 Photovoltaic Cell Engineering Model

A commonly used engineering model for the photovoltaic modules under different temperatures and light conditions is currently available [2]:

$$I = I_{sc} \left\{ 1 - C_1 \left[ \exp \left( \frac{V}{C_2 V_{oc}} \right) - 1 \right] \right\} \quad (1)$$

$$\begin{cases} C_1 = \left( 1 - \frac{I_m}{I_{sc}} \right) \exp \left( -\frac{V_m}{C_2 V_{oc}} \right) \\ C_2 = \left( \frac{V_m}{V_{oc}} - 1 \right) \left[ \ln \left( 1 - \frac{I_m}{I_{sc}} \right) \right]^{-1} \end{cases} \quad (2)$$

$$\left\{ \begin{array}{l} \Delta T = T - T_{\text{ref}} \\ \Delta S = S - S_{\text{ref}} \\ I_{sc} = I_{\text{scref}} \frac{S}{S_{\text{ref}}} (1 + a\Delta T) \\ V_{oc} = V_{\text{ocref}} \ln(e + b\Delta S)(1 - c\Delta T) \\ I_m = I_{\text{mref}} \frac{S}{S_{\text{ref}}} (1 + a\Delta T) \\ V_m = V_{\text{mref}} \ln(e + b\Delta S)(1 - c\Delta T) \end{array} \right. \quad (3)$$

where,  $I_{sc}$ ,  $V_{oc}$ ,  $I_m$ ,  $V_m$  are the short-circuit current, open-circuit voltage, current at the maximum power point and voltage at the maximum power point of the PV module when the actual temperature is  $T$  and the light intensity is  $S$ , respectively.  $I_{\text{scref}}$ ,  $V_{\text{ocref}}$ ,  $I_{\text{mref}}$ ,  $V_{\text{mref}}$  are the short-circuit current, open-circuit voltage, current at the maximum power point, and voltage at the maximum power point under standard conditions, respectively. For  $T_{\text{ref}}$ , the temperature is the standard condition, and  $T_{\text{ref}} = 25^\circ\text{C}$ ;  $S_{\text{ref}} = 1000 \text{ W/m}^2$  and  $S_{\text{ref}}$  indicates the standard light intensity. The coefficients  $a$ ,  $b$ , and  $c$  are constants, where  $a = 0.0025/\text{^\circ C}$ ,  $b = 0.5 \text{ m}^2/\text{W}$ ,  $c = 0.00288/\text{^\circ C}$ .

The engineering model can realize the simulation of PV cells based on their original property parameters suitable for engineering applications. In order to improve the output voltage and power of the photovoltaic power supply in the photovoltaic power generation system, the photovoltaic cells will be connected in series and parallel to form a variety of topologies of photovoltaic arrays. Due to the influence of external environmental factors of the photovoltaic arrays by shadow shading, a long time will be incurred by the hotspot effect, resulting in photovoltaic arrays of the  $U - I$  curve in the form of a ladder,  $U - P$  curves multi-peak, when the engineering model cannot be applied.

## 2.2 Modeling of Photovoltaic Arrays under Localized Shadows

In order to solve the shortcomings of the engineering model, Fu et al. [15] found that the  $I - V$  characteristic curve of the PV cells and the trajectory of the parabolic motion of the mass point had a great similarity to a certain extent, and the kinematic model of the PV monolithic body was constructed by combining the two curves. However, this model only described the output characteristics of the PV array under normal lighting conditions, and the output volt-ampere characteristic curve of the PV array was stepped in the case of shadow shading (Figure 1).

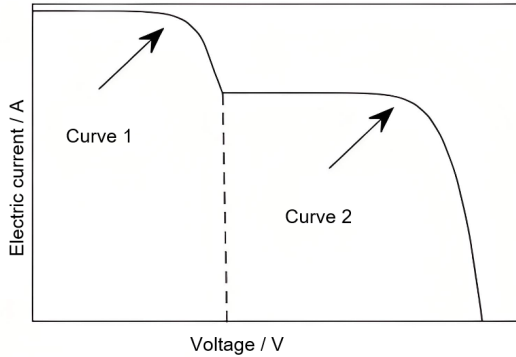


**Figure 1.**  $I - V$  curve of PV array under localized shading

In this paper, the curve was first decomposed into multiple parabolas to simulate the multipoint parabolic motion. The corresponding equations were sequentially derived on the basis of the PV monolithic kinematics model. Finally, each segment of the parabolas was superimposed to derive the model of the PV array under the localized shadow.

Each segment of the parabolic curve can be established in the same coordinate system with the trajectory of the mass parabolic motion, which divides three segments  $(0, xV_m)$ ,  $(xV_m, V_m)$ , and  $(V_m, V_{oc})$  into  $(0, xV_m)$ ,  $(xV_m, V_m)$ ,  $(V_m, V_{oc})$  three segments of the detailed analysis respectively, through the theory of kinematics to deduce the equations of the motion of each segment of the trajectory. Then each segment of the throw is superimposed to arrive at the complete model. The model can accurately capture the change rule of PV array output characteristics under complex shadow shading, effectively solving the limitations of the traditional model in the complex shadow scene. As shown in Figure 2, the horizontal coordinate voltage  $V$  is taken as the movement time of the point, and the vertical coordinate current  $I$  is its displacement in the vertical direction, then the  $I - V$  characteristic curve of the photovoltaic cell can be regarded as the trajectory diagram of the parabolic motion of the point from the position of the point  $(0, I_{sc})$ , and its initial velocity is set as  $V_0$ . In the trajectory of the parabolic motion of the mass point, assume that there are three different gravity fields  $g_0 = 0$  (the mass point is in uniform linear motion),  $g_1$ ,  $g_2$ , and the three gravity fields have the same demarcation as the  $I - V$  characteristic curve. The equation of the gravity field is deduced through kinematics theory, which leads to the equation of the trajectory of the mass point, i.e., the equation of the  $I - V$  characteristic of the photovoltaic array model.

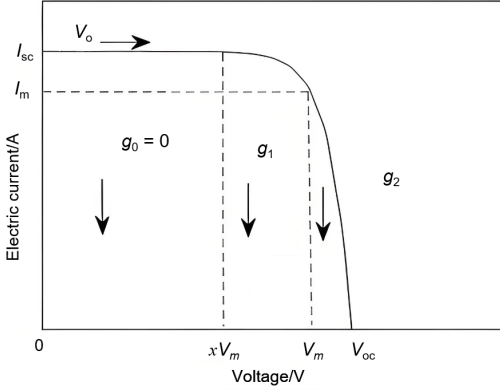


**Figure 2.** Model derivation curve

By analogy with the physical mechanism, we showed that the PV array current-voltage segmentation characteristics had similarity with the acceleration phase of the parabolic motion.

#### Current-Voltage Characteristics of Photovoltaic Arrays

The current of a photovoltaic cell is dominated by photogenerated carriers (photovoltaic current), but its output current is attenuated by internal losses:

- **Constant Current Zone** (Low Voltage Section): The photogenerated current is not significantly canceled, and the output current remains constant, similar to the initial free-fall phase of a parabolic motion, when gravity is the only driving force and the speed increases linearly.
- **Transition Zone** (Medium Voltage Section): As the voltage increases, the reverse saturation current of the PN junction and the loss of the series resistance become progressively more significant and the current decreases nonlinearly. This is analogous to a parabolic motion in which air resistance (proportional to the square of the velocity) begins to cancel out the force of gravity, resulting in a gradual decrease in acceleration.
- **Constant Voltage Zone** (High Voltage Section): As the voltage approaches the open circuit voltage, the photogenerated current is almost completely canceled out by the reverse current and ohmic losses, the current tends to zero and the system stabilizes. Similarly, parabolic motion reaches terminal velocity at the balance between drag and gravity, and acceleration is zero.

#### Acceleration Phase of Parabolic Motion

- **Free-fall phase:** Gravity dominates; acceleration is constant and velocity increases linearly, corresponding to the constant flow region of the PV.
- **Resistance intervention phase:** Air resistance increases with velocity and acceleration decreases, corresponding to the nonlinear decay of the current in the PV transition region.
- **Terminal velocity phase:** Resistance is balanced with gravity; acceleration is zero, and velocity is stabilized, corresponding to current zeroing and voltage saturation in the constant voltage region of the PV.

The theoretical basis for the kinematics of this process of small balls is:

**Stage 1:** ( $V_{ai-1} \leq V < XV_{mi}$ ), since the driving force is provided by the current  $I_{ai}$ , the resistance is neglected, i.e.  $F = k \sum I_{ai}$ , where  $k$  is the conversion factor, so there is Newton's second law:

$$a = \frac{F_{\text{driving}}}{m} = \frac{k}{m} \sum_{i=1}^n I_{ai} \quad (4)$$

**Stage 2:** Secondary Resistance Intervention ( $XV_{mi} \leq V \leq V_{mi}$ ). The driving force remains  $\sum I_{ai}$ , but when the velocity exceeds the threshold  $XV_{mi}$ , the resistance is proportional to the velocity squared, so:

$$F_{\text{resistance}} = \frac{1}{2} g_1 \left( \frac{V - XV_{mi}}{V_i} \right)^2 \quad (5)$$

According to Newton's second law, acceleration is determined by the net external force, hence Newton's law:

$$a = \frac{F_{\text{total}}}{m} = \frac{F_{\text{driving}} - F_{\text{resistance}}}{m} \quad (6)$$

Substitute drive and drag expressions:

$$\frac{dV}{dt} = \frac{k}{m} \sum_y^x I_{ai} - \frac{g_1}{2m} \sum_{i=1}^n \left( \frac{V - XV_{mi}}{V_i} \right)^2 \quad (7)$$

**Stage 3:** Linear Resistance Dominance ( $V_{mi} \leq V \leq V_{ai}$ ): when the speed approaches the preset maximum threshold  $V_{mi}$ , the system actively reduces the drive current to prevent overshooting or overheating. The drive switches from  $I_{ai}$  to  $I_{mi}$ , i.e.:

$$F_{\text{driving}} = k \sum_{i=1}^n I_{mi} \quad (8)$$

At this time, the resistance model is a combination of linear terms cross terms, linear resistance, the velocity close to  $V_{mi}$ , resistance and velocity difference linear correlation, cross resistance terms, inherited stage two of the quadratic resistance effect, the transition to linear resistance, then there are:

$$F_{\text{resistance,linear}} = \frac{1}{2} g_2 \sum_{i=1}^n \left( \frac{V - V_{mi}}{V_i} \right) \quad (9)$$

$$F_{\text{resistance,cross}} = g_1 \sum_{i=1}^n \left( \frac{(1-X)V_{mi}}{V_i} \cdot \frac{V - V_{mi}}{V_i} \right) \quad (10)$$

According to Newton's second law, acceleration is determined by the net external force:

$$a = \frac{F_{\text{total}}}{m} = \frac{F_{\text{driving}} - (F_{\text{resistance, linear}} + F_{\text{resistance, cross}})}{m} \quad (11)$$

Substituting the specific expression, we have:

$$\frac{dV}{dt} = \frac{k \sum_{i=1}^n I_{mi}}{m} - \frac{1}{m} \left[ \frac{g_2}{2} \sum_{i=1}^n \left( \frac{V - V_{mi}}{V_i} \right) + g_1 \sum_{i=1}^n \left( \frac{(1-X)V_{mi}}{V_i} \right) \right] \quad (12)$$

where,  $V$  is the velocity of the ball movement,  $I$  is the equivalent drive current,  $V_{ai-1}, V_{ai}$  are the  $k$  boundaries of the velocity intervals (e.g., initial and termination velocities),  $V_{mi}$  is the maximum velocity threshold at  $i$ ,  $X$  is the scaling coefficient,  $k$  is the conversion coefficient,  $g_1, g_2$  are the resistance coefficients, and  $V_i$  is the reference velocity.

From the theory of kinematics, one can derive the equation of the trajectory of the ball:

$$I = \begin{cases} \sum_{i=1}^n I_{sc_i}, & (V_{oc_{i-1}} \leq V < X_i V_{mi}, V_{oc_0} = 0) \\ \sum_{i=1}^n \left[ I_{sc_i} - \frac{1}{2} g_{i1} \left( \frac{V - X_{ij} V_{ij}}{V_i} \right) \right], & (X_i V_{mi} \leq V < V_{mi}) \\ \sum_{i=1}^n \left[ I_{mi} - \frac{1}{2} g_{i2} \left( \frac{V - V_{mi}}{V_i} \right) - g_{i1} \left( \frac{V_{in} - X V_{mi}}{V_i} \right) \left( \frac{V - V_{mi}}{V_i} \right) \right], & (V_{mi} \leq V < V_{oc_i}) \end{cases} \quad (13)$$

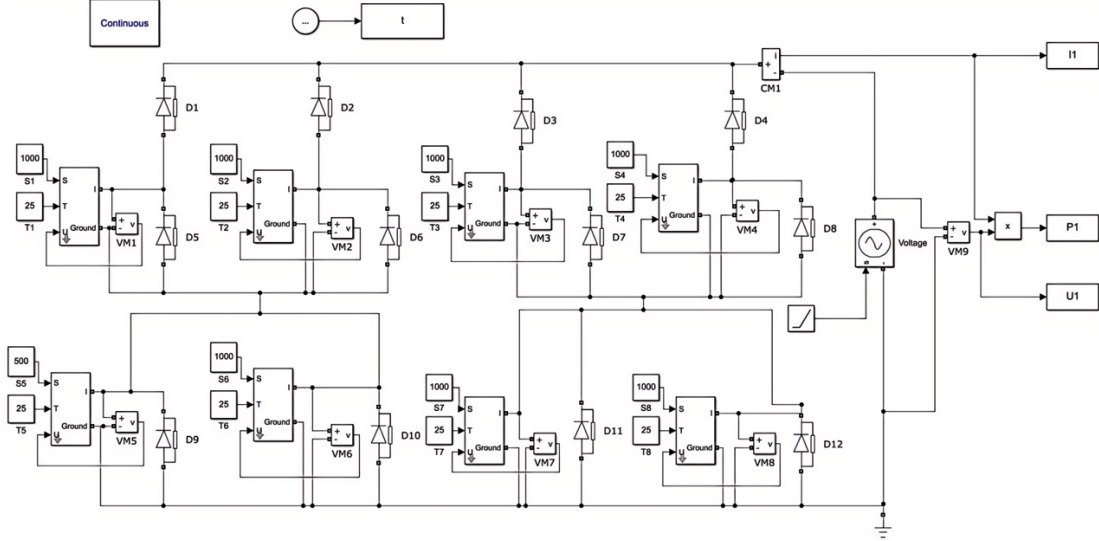
where, the values of  $g_{i1}$  and  $g_{i2}$  are as follows:

$$\begin{cases} g_{i1} = \frac{2(I_{sc_i} - I_{mi})V_i^2}{(V_{mi} - X_i V_{mi})^2} \\ g_{i2} = \frac{2V_i^2 I_{mi} (V_{mi} - X_i V_{mi}) - 4V_i^2 (I_{sc_i} - I_{mi}) (V_{oc_i} - V_{mi})}{(V_{mi} - X_i V_{mi}) (V_{oc_i} - V_{mi})^2} \end{cases} \quad (14)$$

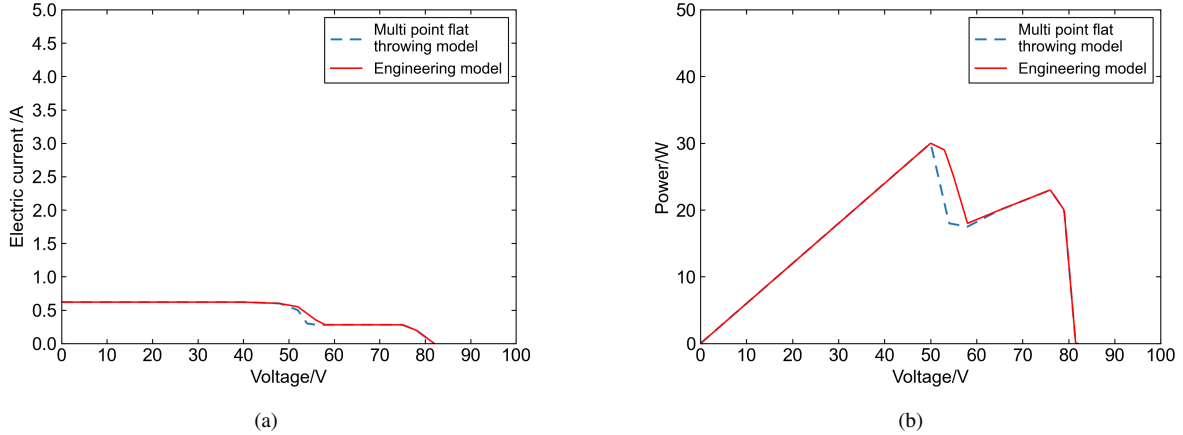
where,  $I_{sc_i}, V_{oc_i}, I_{mi}, V_{mi}$  are the short-circuit current, open-circuit voltage, current at the maximum power point and voltage at the maximum power point of the PV module when the light intensity is  $S$ , respectively, and  $(n-1)$  is the number of modules shaded by the shadow. Fu et al. [15] concluded from a comparative analysis of a large number of measured data that both monocrystalline silicon and polycrystalline silicon solar cells, under the general environmental conditions of terrestrial light and temperature, the value of  $x$  is positively correlated with the intensity of light, and has little relationship with the cell temperature, and then fitted the formula for the optimal value of  $x$  as:  $x = 0.00027 S + 0.5492$ . This formula is generalized for models based on parabolic motion, and the model proposed in this paper is also derived based on parabolic motion, so the value of  $x$  in the model of this paper is the same as above.

### 3 Simulation Verification

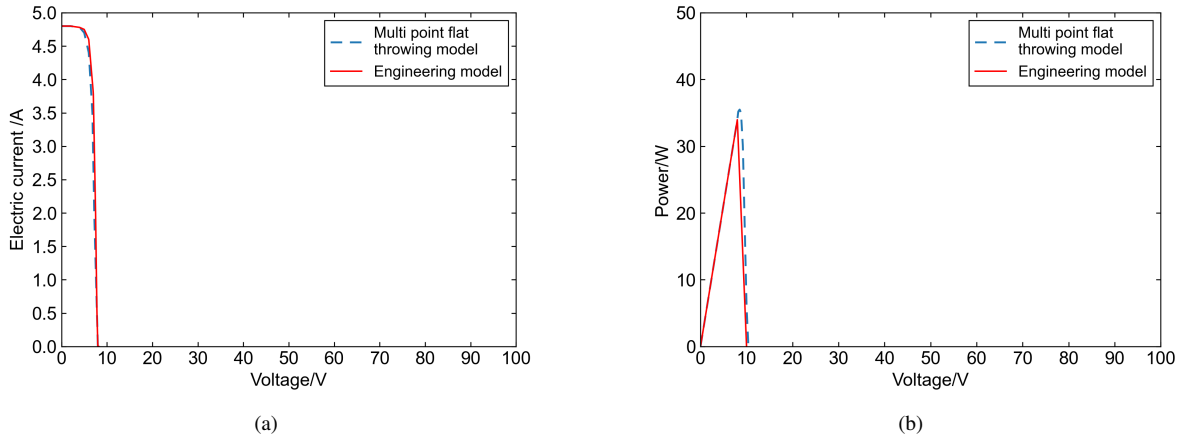
In order to verify the superiority and applicability of the model established in this paper, PV arrays with various topologies (series, parallel, SP, TCT, and CTCT) were constructed in MATLAB/Simulink, in which CTCT arrays (each row of PV modules is connected in parallel first, and then connected in series between rows, and then a group of modules are connected in parallel again, and then continue to be connected in series) were simulated. The specific number of series and parallel connections was determined according to the actual situation [16] simulated in Figure 3.



**Figure 3.** Simulation of CTCT array



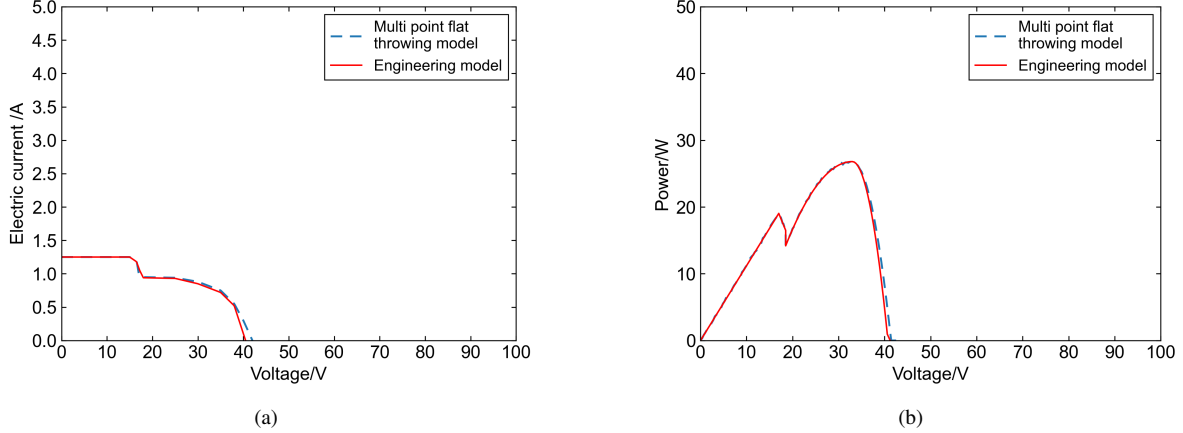
**Figure 4.** Tandem array: (a) voltage-current comparison plot; (b) voltage-power comparison plot



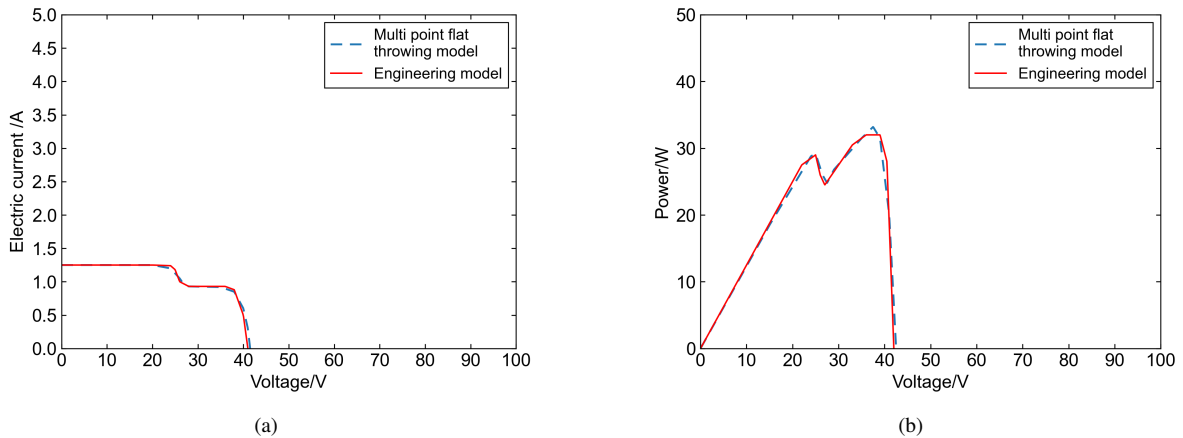
**Figure 5.** Parallel array: (a) voltage-current comparison plot; (b) voltage-power comparison plot

Figure 4, Figure 5, Figure 6, Figure 7 and Figure 8 show the voltage-current and voltage-power curves of the engineering model and the multipoint parabolic model. The basic parameters of a single PV module are the same as the performance parameters of the PV panels measured later:  $V_{oc} = 10.2$  V,  $I_{sc} = 0.62$  A,  $V_m = 9$  V,  $I_m = 0.56$  A.

The reference temperature is: 25°C, the reference illumination is: 1000 W/m<sup>2</sup>, and the blocking part of the illumination is: 500 W/m<sup>2</sup>. From the charts of voltage-current and voltage-power comparison, it can be seen that the multipoint parabolic model value and the engineering model value are slightly different, but the error is within the permissible accuracy 5% of engineering. The output curves basically overlap and the power curves of the two models have the same wave peaks.



**Figure 6.** SP array: (a) voltage-current comparison plot; (b) voltage-power comparison plot



**Figure 7.** TCT array: (a) voltage-current comparison plot; (b) voltage-power comparison plot

The current equation model of PV arrays under localized shadowing conditions established by Liu et al. [17] is applicable to PV arrays with simple structures under shadowing conditions. The voltage-current and voltage-power curves of this model and the engineering model, and the multipoint parabolic model under series and SP structures are shown in Figure 9 and Figure 10. As for the voltage-current curves, the engineering model and the multipoint parabolic model are nearly coincidental, and the trend of current change is consistent, hence providing reliable results, while the current equation model is obviously deviated from the key voltage nodes and the amplitude of the current change varies greatly, resulting in larger simulation errors. As for the voltage-power curve, the engineering model and the multipoint parabolic model have similar location and value of the maximum power point, which can effectively guide the practical application, while the current equation model has low value and deviation of the maximum power point, which is obviously insufficient to describe the power output characteristics. Since the voltage in the current equation model depends on the maximum value of the voltage of each column of the PV array, this leads to an error in the value of the voltage in the shading part. In addition, since the current in this model is calculated by dividing each column into two segments, the corresponding PV array has at least two PV modules in series, which makes it impossible to accurately describe complex PV arrays such as parallel, TCT, and CTCT if they are encountered. Therefore, the multipoint parabolic model simulates with high accuracy and consistency, and the current equation model is so limited that it is difficult to provide accurate and reliable results.

In order to further verify the advancement of the model in this paper, the reconstruction strategy proposed by

Zhu et al. [13] was introduced as a benchmark for comparison. As shown in Figure 11, this strategy optimizes the output power through the 0–1 multiple backpack problem relied on the principle of irradiance equalization. The magnitude of power fluctuation under dynamic shadowing was significantly higher than that of the model in this paper. In addition, the elapsed time of its computation was far more than that of the current model, which further confirms the advantage of the proposed method in real time.

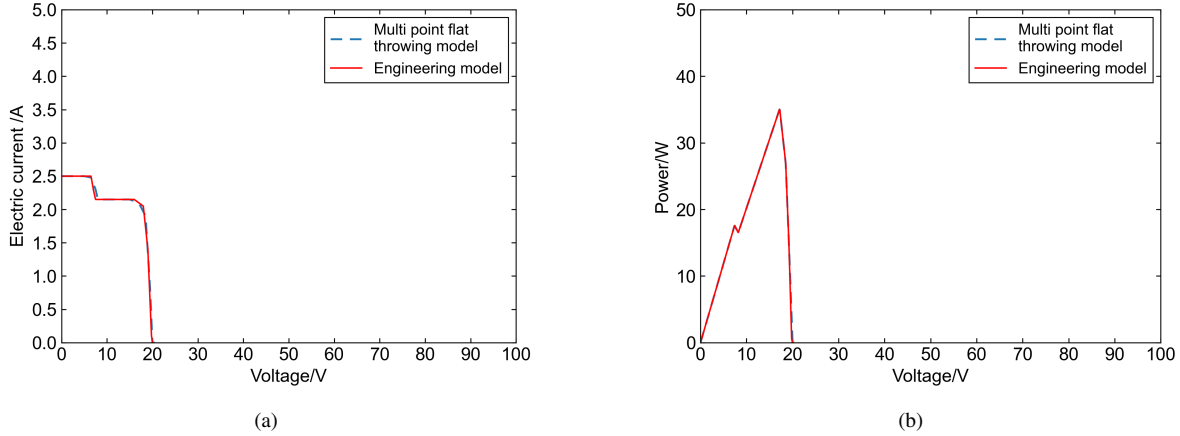


**Figure 8.** CTCT array: (a) voltage-current comparison plot; (b) voltage-power comparison plot

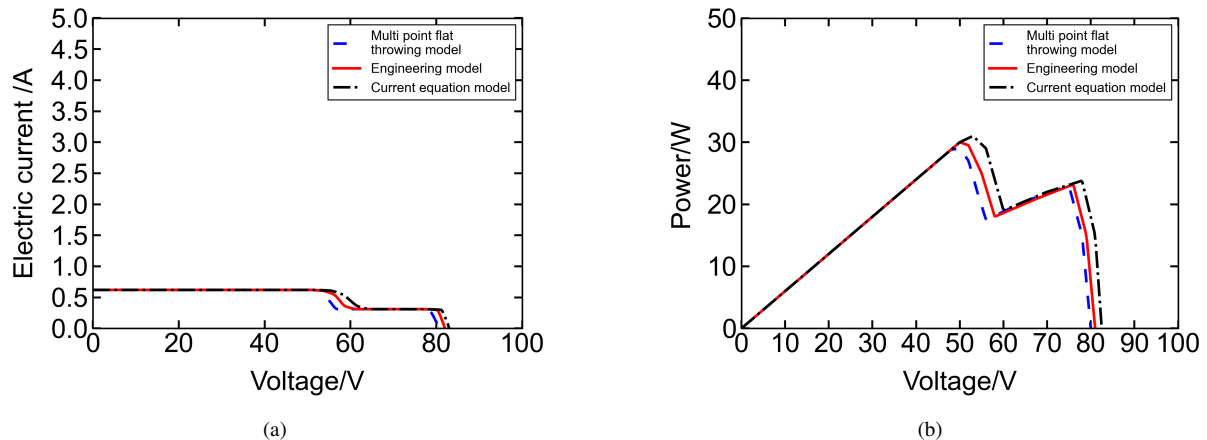


**Figure 9.** Tandem array: (a) voltage-current comparison plot; (b) voltage-power comparison plot

**Table 1.** Comparison of the three models  $U_m$ ,  $I_m$

	Engineering Model		Current Equation Modeling		Multipoint Parabolic Model	
	$U_m$ /V	$I_m$ /A	$U_m$ /V	$I_m$ /A	$U_m$ /V	$I_m$ /A
Establish ties or contact	50	0.592	52.4	0.585	51.15	0.584
Parallel connection	7.5	4.535	×	×	7.837	4.427
SP	32.5	0.822	27.4	0.889	31.54	0.851
TCT	37.5	0.872	×	×	37.76	0.871
CTCT	17	2.049	×	×	17.19	2.047
Computation time	4 s		0.237348 s		0.113692 s	

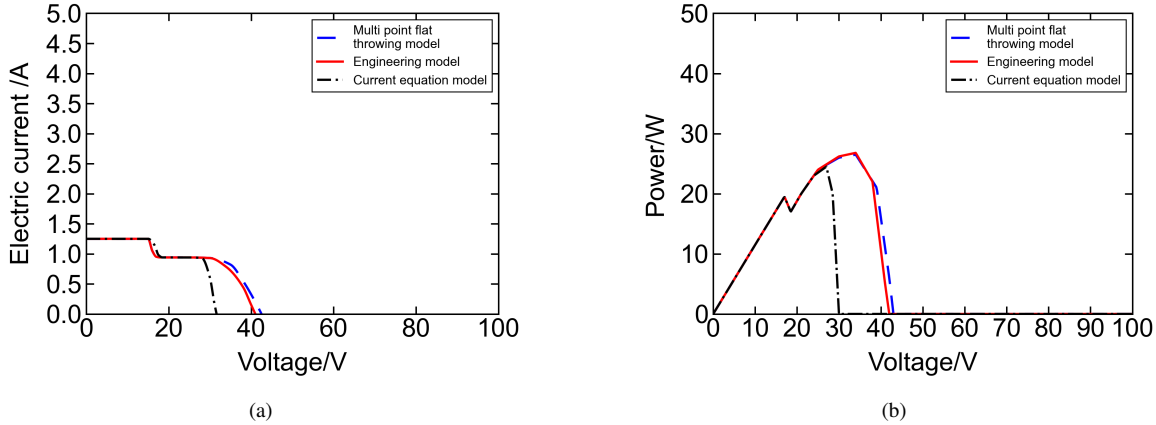


**Figure 10.** SP array: (a) voltage-current comparison plot; (b) voltage-power comparison plot

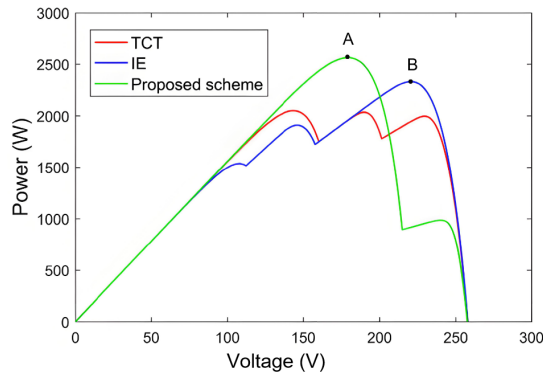


**Figure 11.** Curves of Power-Voltage (P-V) characteristic

**Table 2.** Comparison of the error in each model with the engineering model,  $U_m$

	In-Series Connection (Electricity)	Parallel Connection	SP	TCT	CTCT
Current Equation Modeling	4.8%	×	15.7%	×	×
Multipoint Parabolic Model	2.3%	4.5%	2.9%	0.6%	1.1%

In practice, the maximum power point of the PV cell shifts with atmospheric conditions [18], so the operating voltage of the system must be adjusted in real time so that the array can work at the maximum power point at any moment and output the most amount of power to the outside world. Table 1 and Table 2 present the comparison table of  $U_m$  and  $I_m$  for the three models (i.e., engineering model, current equation model, and multipoint parabolic model), and the comparison table of  $U_m$  error between each model and the engineering model, respectively.

It can be clearly seen from the comparison that the voltage and current values where the maximum power point of the current equation model is located have a larger offset, compared with the engineering model which has an impact on the adjustment of the operating voltage corresponding to the maximum power real-time output of the photovoltaic power plant. The voltage and current parameters corresponding to the maximum power point of the multipoint parabolic model and the engineering model are almost the same. Since the engineering model involves exponential operations, the calculation is cumbersome and complex. The model proposed in this paper, on the premise that the error reaches 5% or less, significantly reduces the calculation amount compared with the engineering model, and the solution is simpler. It is therefore possible to quickly and accurately calculate the output characteristics of PV arrays in the face of arbitrary shading patterns such as different light intensities, different shading locations and areas, etc., thus providing robust support for real-time monitoring of PV systems, maximum power tracking and control, and other practical applications which greatly improves the operational efficiency and stability of PV systems. Shading is a temporary fault that requires dynamic modeling support, and the model in this paper is segmentally fitted by

parabolic motion, and can successfully capture the multi-peak characteristics under dynamic shading. In addition, the multipoint parabolic model constructed in this paper has a wide range of applications, which is not only limited to series-parallel, SP, and TCT structures, but also applicable to other complex PV array structures.

#### 4 Hotspot Simulation Platform Measurement and Analysis

In order to verify the accuracy of the proposed model, a hotspot simulation platform consisting eight PV panels, current input distribution isolator module, signal acquisition module, and control module was constructed. The block diagram of the hardware circuit is shown in Figure 11.

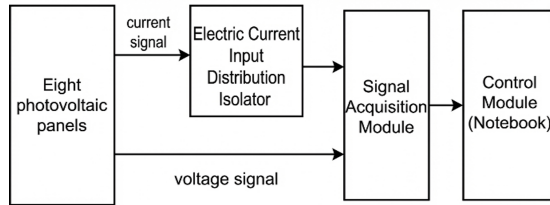


**Figure 12.** Diagram of hardware circuit block



**Figure 13.** Simulated hotspot platform

Each photovoltaic panel was connected to the relay through the control of the relay on and off to realize the transformation of the topology of the photovoltaic array. The platform used the MY1521 current input distribution isolator, whose function is to isolate the direct current (DC) signal output from the photovoltaic array, and then converted to a standard voltage signal. The output current and output voltage collected through the current input distribution isolator entered the control module (laptop) through the signal acquisition module, as shown in Figure 12.

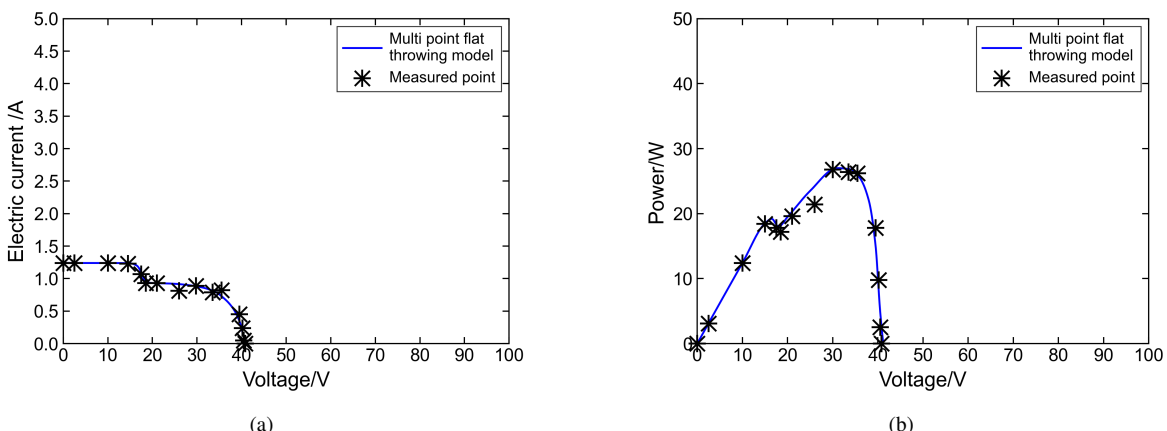


**Figure 14.** SP array: (a) voltage-current comparison plot; (b) voltage-power comparison plot

The hotspot fault was simulated by shading half of the area of PV panel No. 1 during the experiment, and the

output current and voltage of the PV array under the SP, TCT, and CTCT structures were measured respectively. The voltage-current and voltage-power curves of the multipoint parabolic model were compared with the experimentally measured data as shown in Figure 13, Figure 14 and Figure 15.

From the figures, it can be seen that the theoretical output curve of the derived model is slightly different from the experimentally measured data. The maximum power point voltage  $U_m$  of the multipoint parabolic model is consistent with the measured data of the PV arrays with SP and TCT structures; it is improved by 3% compared with the measured data of the PV arrays with CTCT structure. This is due to the fact that the theoretical model is derived under the ideal conditions, thereby ignoring the loss of diodes inside the PV panels and the effect of temperature changes during the experiment. The trend of most of the measured points is consistent with the theoretical curve. Therefore, the multipoint parabolic model proposed in this paper can accurately describe the output characteristics of complex PV arrays under shadow shading.

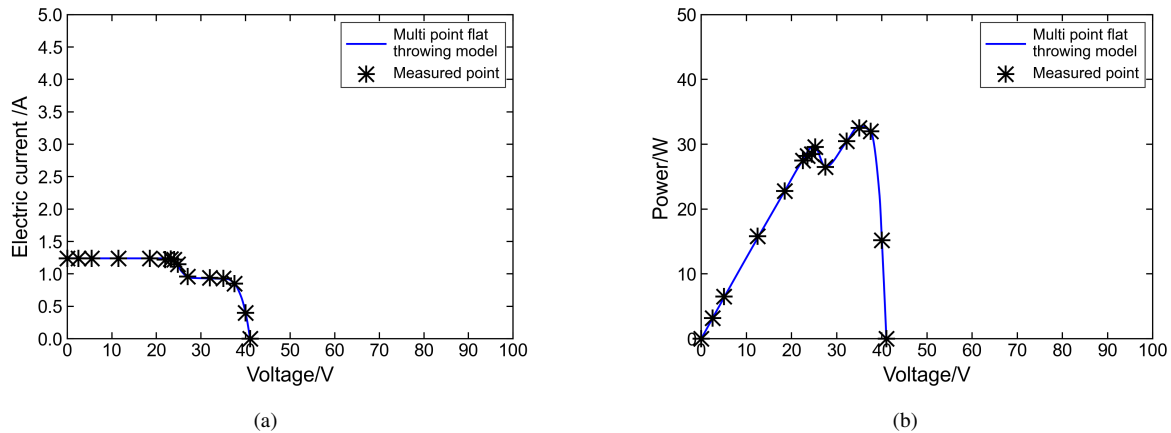


**Figure 15.** TCT array: (a) voltage-current comparison plot; (b) voltage-power comparison plot

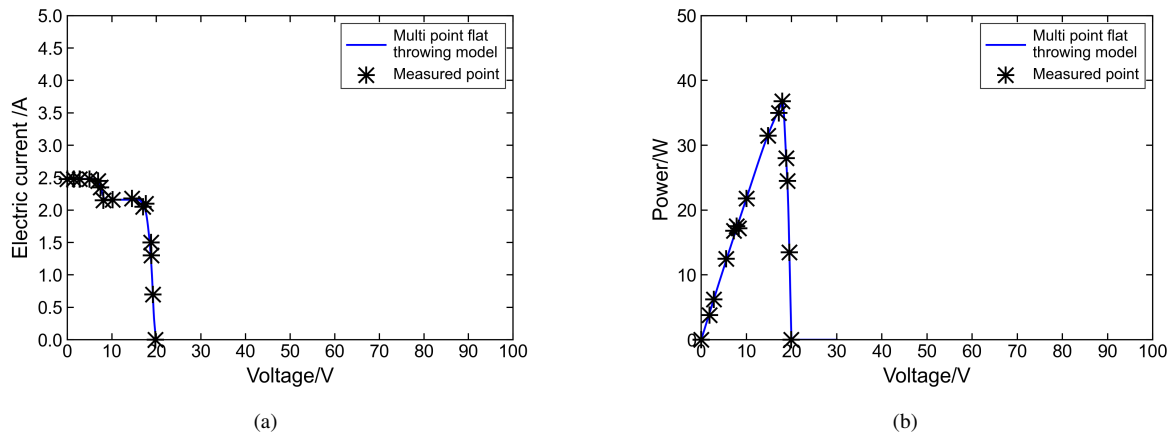


**Figure 16.** CTCT array: (a) voltage-current comparison plot; (b) voltage-power comparison plot

**Table 3.** Comparison of  $V_m$  error under different topologies

Item	SP (V)	TCT (V)	CTCT (V)
Measured value	31.51	37	16.68
Multipoint parabolic model	31.54	37	17.19
Error	0.04%	0%	3%

From the results of the comparison in Figure 16, it can be seen that there are some numerical differences between the measured data and the theoretical output curves of the multi-parabolic model. The curves of the output

characteristics of measured data trajectory have the same wave peaks. Comparing the model-derived maximum power point voltage with the results obtained from the real measurements, the results are shown in Table 3.

## 5 Conclusions

This paper combined the PV monolithic engineering model and the kinematic model to establish a multipoint parabolic motion PV array model under localized shadowing conditions. Simulation and experimental verification were performed to analyze the output characteristics of the proposed model under localized shadowing conditions. When compared with the engineering model and other improved models, the currently proposed model can be applied to the modeling of complex topology PV arrays under local shadowing conditions. The curve of the output characteristics of the present model has an error of less than 5% in comparison with the engineering model, thus providing theoretical and experimental bases for the study of maximum power tracking of PV systems and reducing the loss of PV system output power. Although the model in this paper has been significantly optimized in terms of computational efficiency, there is still a large room for improvement. In the future, it can be combined with deep learning [19] to apply multimodal data to further improve the accuracy of fault diagnosis under dynamic shadowing. By integrating the bending characteristics of flexible PV arrays [20] with the shadow shading model in this paper, the optimization of PV systems under multi-physics field coupling can be explored. Moreover, further integration of physical modeling and machine learning techniques is also possible. Using the multipoint parabolic model in this paper as a feature extraction tool, combined with the Artificial Neural Network (ANN) framework proposed by Zwirtes et al. [21], a hybrid fault diagnosis system could be constructed. This could help retain the accurate description of multi-peak characteristics of the physical model, take advantage of machine learning to generalize dynamic shading and unknown faults, and enhance the efficiency of real-time monitoring of the PV system.

## Author Contributions

Conceptualization, Z.K.D. and G.C.; methodology, Z.K.D., C.L., and Z.C.; software, Z.K.D. and Y.Z.; validation, C.L., W.W., R.M., X.Y.W., J.Q.W., and Z.P.Y.; formal analysis, Z.K.D., W.W., and Z.Y.Y.; investigation, J.Q.W., R.M., X.Y.W., Y.Z., and Z.P.Y.; resources, G.C.; data curation, R.M., J.Q.W., and Z.P.Y.; writing—original draft preparation, Z.K.D.; writing—review and editing, G.C., Z.Y.Y., Y.S.S., and H.C.Z.; visualization, D.Y.L., H.C.Z., and Z.K.D.; supervision, G.C.; project administration, G.C.; funding acquisition, G.C. All authors have read and agreed to the published version of the manuscript.

## Funding

This article was funded by Research Project No. XYN1805 of Jiangsu Universities Collaborative Innovation Center for Cultural and Creative Industries, Nanchang Hangkong University Ministry of Education Key Laboratory of Non-Destructive Testing Technology Open Fund (Grant No.: EW201980089), and University-Industry Collaborative Education Program in the Ministry of Education (Grant No.: 20192156019 and Grant No.: 201902156031).

## Data Availability

The data used to support the findings of this study are available from the corresponding author upon request.

## Conflicts of Interest

The authors declare that they have no conflicts of interest.

## References

- [1] S. Boubaker, S. Kamel, N. Ghazouani, and A. Mellit, “Assessment of machine and deep learning approaches for fault diagnosis in photovoltaic systems using infrared thermography,” *Remote Sens.*, vol. 15, no. 6, p. 1686, 2023. <https://doi.org/10.3390/rs15061686>
- [2] X. R. Wang and D. X. Bian, “Modeling and characterization of photovoltaic arrays under local shadows,” *Mod. Electron. Technol.*, vol. 42, no. 8, pp. 109–112+117, 2019. <https://doi.org/10.16652/j.issn.1004-373x.2019.08.024>
- [3] C. Shao, A. Migan-Dubois, and D. Diallo, “Performance of PV array configurations under dynamic partial shadings,” *EPJ Photovolt.*, vol. 14, p. 21, 2023. <https://doi.org/10.1051/epjpv/2023012>
- [4] G. G. Kim, W. Lee, B. G. Bhang, J. H. Choi, and H. K. Ahn, “Fault detection for photovoltaic systems using multivariate analysis with electrical and environmental variables,” *IEEE J. Photovolt.*, vol. 11, no. 1, pp. 202–212, 2020. <https://doi.org/10.1109/JPHOTOV.2020.3032974>
- [5] G. L. Li, F. Wang, F. Feng, and B. Wei, “Hot spot detection of photovoltaic module based on distributed fiber Bragg grating sensor,” *Sensors*, vol. 22, no. 13, p. 4951, 2022. <https://doi.org/10.3390/s22134951>
- [6] L. El Iysaouy, M. Lahbabi, K. Bhagat, M. Azeroual, Y. Boujoudar, H. Saad El Imanni, A. Aljarbouh, A. Pupkov, M. Rele, and S. Ness, “Performance enhancements and modelling of photovoltaic panel configurations during partial shading conditions,” *Energy Syst.*, pp. 1–22, 2023. <https://doi.org/10.1007/s12667-023-00627-7>

- [7] T. T. Pei and X. H. Hao, "Dynamic modeling of photovoltaic arrays under local shadowing conditions," *J. Sol. Energy*, vol. 41, no. 2, pp. 274–280, 2020. <https://doi.org/10.19912/j.0254-0096.2020.02.039>
- [8] Y. N. Chanchangi, A. Ghosh, S. Sundaram, and T. K. Mallick, "Dust and PV performance in Nigeria: A review," *Renew. Sustain. Energy Rev.*, vol. 121, p. 109704, 2020. <https://doi.org/10.1016/j.rser.2020.109704>
- [9] Y. N. Chanchangi, A. Ghosh, S. Sundaram, and T. K. Mallick, "An analytical indoor experimental study on the effect of soiling on PV, focusing on dust properties and PV surface material," *Sol. Energy*, vol. 203, pp. 46–68, 2020. <https://doi.org/10.1016/j.solener.2020.03.089>
- [10] A. Almarri, R. AlMutairi, F. Alnass, N. Alghamdi, M. M. Ghobashy, M. S. Attia, and M. Madani, "Experimental and modeling study of dust composition impact on photovoltaic performance in arid coastal environments," *J. Mater. Res. Technol.*, vol. 39, pp. 5455–5467, 2025. <https://doi.org/110.1016/j.jmrt.2025.10.169>
- [11] M. Parvin, H. Yousefi, and B. Mohammadi-Ivatloo, "Photovoltaic fault detection algorithm using ensemble learning enhanced with deep neural network feature engineering," *Results Eng.*, vol. 27, p. 106491, 2025. <https://doi.org/10.1016/j.rineng.2025.106491>
- [12] K. Tai, C. Mo, and C. Hang, "Influence of local shadow on output of photovoltaic array," *J. Phys.: Conf. Ser.*, vol. 2087, no. 1, p. 012015, 2021. <https://doi.org/10.1088/1742-6596/2087/1/012015>
- [13] Z. Zhu, M. Hou, L. Ding, G. Zhu, and Z. Jin, "Optimal photovoltaic array dynamic reconfiguration strategy based on direct power evaluation," *IEEE Access*, vol. 8, pp. 210 267–210 276, 2020. <https://doi.org/10.1109/ACCESS.2020.3036124>
- [14] G. M. El-Banby, N. M. Moawad, B. A. Abouzalm, W. F. Abouzaid, and E. A. Ramadan, "Correction to: Photovoltaic system fault detection techniques: A review," *Neural Comput. Appl.*, vol. 36, no. 29, pp. 18 547–18 548, 2024. <https://doi.org/10.1007/s00521-024-10056-x>
- [15] W. Fu, L. Zhou, K. Guo, Q. Liu, and L. Dai, "On the digital PV array simulator based on horizontal projectile motion," *East China Electr. Power*, vol. 39, no. 3, pp. 468–473, 2011.
- [16] W. H. Song, T. Z. Li, J. Z. Qiao, J. Z. Cui, and P. H. Jiao, "Research on the fault detection method of TCT-structured photovoltaic arrays," *Power Technol.*, vol. 43, no. 7, pp. 1164–1167, 2019.
- [17] X. Y. Liu, X. M. Qi, S. S. Zheng, D. M. Chen, and F. Wang, "Research on the simulation model of photovoltaic arrays under localized shadowing conditions," *J. Syst. Simul.*, vol. 24, no. 5, pp. 1125–1131, 2012. <https://doi.org/10.16182/j.cnki.joss.2012.05.021>
- [18] H. Deboucha, M. Kermadi, S. Mekhilef, and S. L. Belaid, "Ultra-fast and accurate MPPT control structure for mobile PV system under fast-changing atmospheric conditions," *IEEE Trans. Sustain. Energy*, vol. 14, no. 4, pp. 2168–2176, 2023. <https://doi.org/10.1109/TSTE.2023.3260031>
- [19] S. Afrasiabi, S. Allahmoradi, M. Afrasiabi, X. Liang, C. Y. Chung, and J. Aghaei, "A robust multi-modal deep learning-based fault diagnosis method for PV systems," *IEEE Open Access J. Power Energy*, 2024. <https://doi.org/10.1109/OAJPE.2024.3497880>
- [20] G. Chen, Y. Wang, Y. Xu, Y. Zhu, J. Li, W. Wang, and X. Li, "Study on electrical characteristics of thin flexible crystalline silicon solar cells," *J. New Mater. Electrochem. Syst.*, vol. 25, no. 1, 2022. <https://doi.org/10.14447/jnmes.v25i1.a11>
- [21] J. Zwirtes, F. Bastos Líbano, L. A. de Lima Silva, and E. Pignaton de Freitas, "Fault detection in photovoltaic systems using a machine learning approach," *IEEE Access*, vol. 13, pp. 41 406–41 421, 2025. <https://doi.org/10.1109/ACCESS.2025.3547838>